Infrared studies of comets

Infrared spectrum of comet C/1995 O1 (Hale-Bopp) in 1997

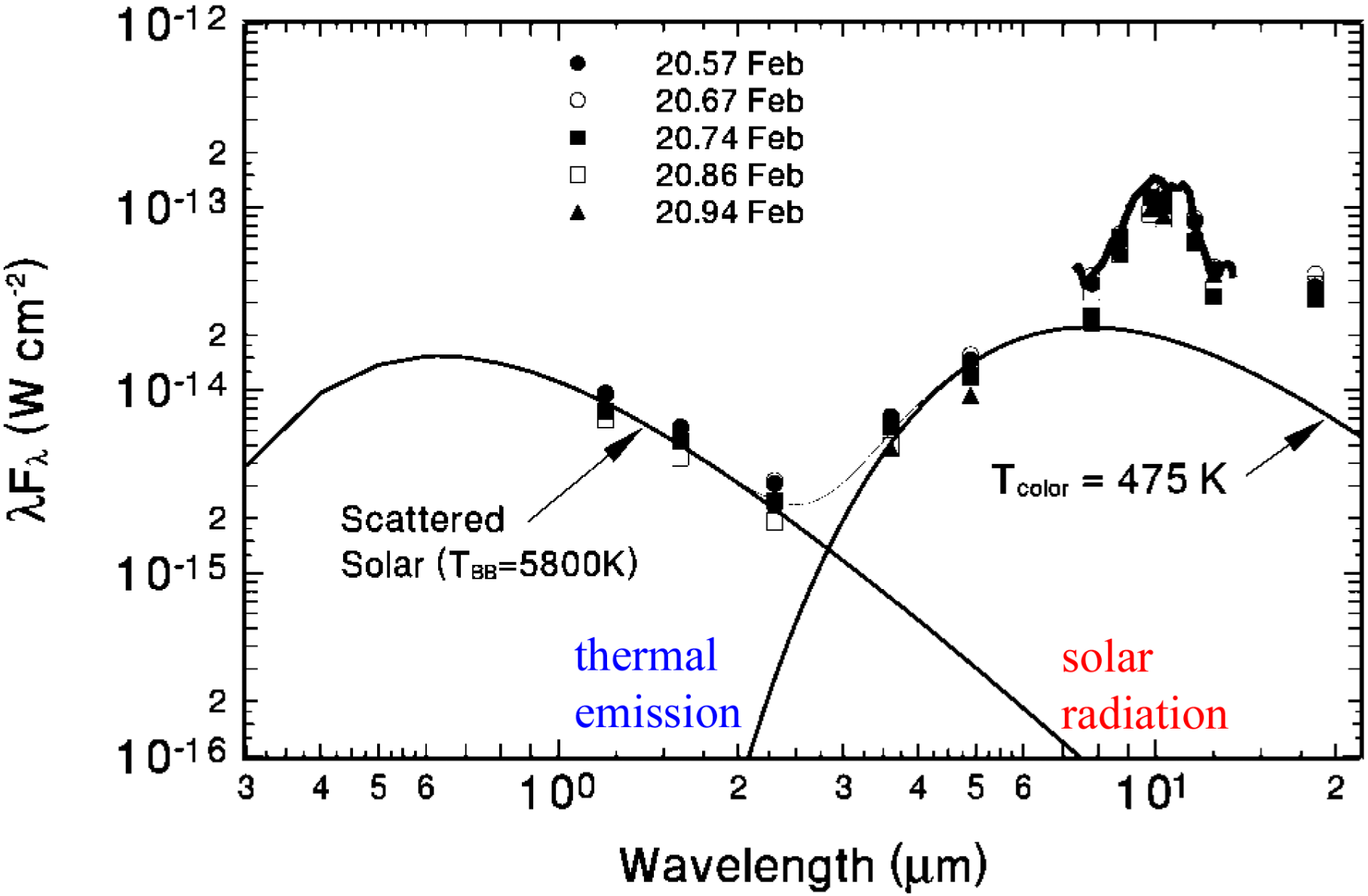

At wavelength λ less than 3 – 4 μm, the spectrum of a comet is dominated by the scattered sun-light; whereas, at larger λ, it is caused basically by thermal emission, coming from the heated cometary grains.

Interpretation of the infrared spectrum is based on the black body model (a body with absorptivity a = 1.0). By fitting of mid-infrared spectrum of a comet with black body model, one can obtain the color temperature of cometary grains T_c.

According to Wien's displacement law:

$$\lambda_{max} = b/T_c,$$

where, b = 0.002899 (m K) and T_c is the color temperature (measured in Kelvin).

Note that the color temperature T_c is not a physical temperature.

The Wien's displacement law

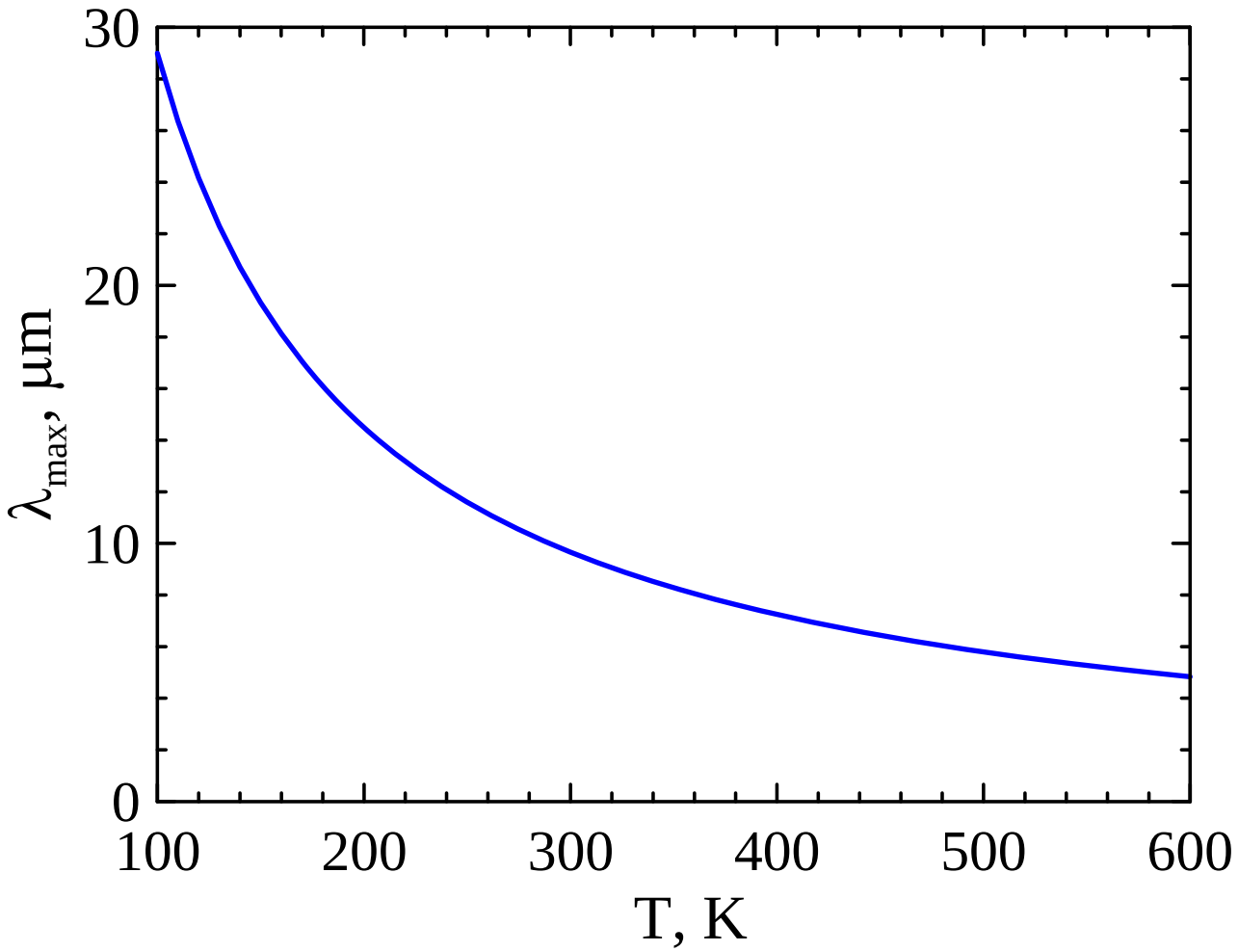

λ_{max}= 5 μm: T=580 K

λ_{max}=10 μm: T=290 K

λ_{max}=15 μm: T=195 K

λ_{max}=20 μm: T=140 K

λ_{max}=25 μm: T=115 K

While the Wien's displacement law fits only λ_{max}, one can try to fit the full mid-infrared spectrum with the Planck's law:

$$B(\lambda, T) = \frac{2hc^2}{\lambda^5} \frac{1}{e^{\frac{hc}{\lambda k T}} - 1}$$

where, λ is wavelength, T – the color temperature, Planck constant – $h = 6.626 \times 10^{-34}$ J · s, speed of light – $c = 3 \times 10^9$ m/s, and Boltzmann constant – $k = 1.38 \times 10^{-23}$ J/K.

However, the fitting with the Planck's law can be done for only quite simple targets (cloud of identical dust particles); whereas, in the case of complex comae, this approach will obviously fail.

Number of outstanding maxima in the mid-infrared spectrum is equal to number of components in cometary coma.

As was already pointed out, the color temperature does not correspond to physical temperature of dust grains.
So, what is the benefit from knowing the color temperature?

Using the color temperature, one can derive the total energy radiated per unit surface area of a black body per unit time (i.e., energy flux density) from the Stefan–Boltzmann law:

$$j = \sigma T^4,$$

where, the Stefan–Boltzmann constant $\sigma = 5.67 \times 10^{-8}$ J s m^{-2} K^{-4}.

Once the energy flux density is known, from the mid-infrared measurements of a comet, one can estimate the area of emitting surface.

Notice, in the case of a grey body, the Stefan–Boltzmann law is being modified through an extra factor ε (emissivity).

How to compute the emissivity ε of a grey body?

One can do that with help of the Kirchhoff's law of thermal radiation.

For arbitrary body, the absorptivity a and emissivity ε are complex functions of variables λ and T, as well as other properties of the target. However, the ratio of emissivity ε over absorptivity a is the same function of λ and T, for all the bodies.

If so, than the same also holds true for a black body, which absorptivity $a(\lambda, \mathrm{T}) = 1$ and emissivity $\varepsilon(\lambda, \mathrm{T}) = \mathrm{B}(\lambda, \mathrm{T})$.

Taking into account that, in light scattering theory, absorptivity a is equivalent to the cross section for absorption C_{abs}, one can formulate:

$$\frac{\varepsilon(r, m, \lambda, \mathrm{T})}{C_{abs}(r, m, \lambda)} = \mathrm{B}(\lambda, \mathrm{T})$$

Therefore, the emissivity ε can be computed as follows:

$$\varepsilon(r, m, \lambda, \mathrm{T}) = \mathrm{B}(\lambda, \mathrm{T})\, C_{abs}(r, m, \lambda)$$

Once the emissivity is known, one can compute the physical temperature of cometary dust grains being under thermal equilibrium, as follows:

$$\frac{1}{R^2} \int C_{abs}(r, m, \lambda)\, \mathrm{E}_{\mathrm{o}}(\lambda)\, G\, d\lambda = \int \varepsilon(r, m, \lambda, \mathrm{T})\, S\, d\lambda$$

where, $\mathrm{E}_{\mathrm{o}}(\lambda)$ – the solar radiation flux at 1 A.U., R – heliocentric distance (in A.U.), G and S – geometric cross section and surface area of dust particle, ε – emissivity. Or, taking into account expression for emissivity:

$$\frac{1}{R^2} \int C_{abs}(r, m, \lambda)\, \mathrm{E}_{\mathrm{o}}(\lambda)\, d\lambda = \frac{S}{G} \int \pi \mathrm{B}(\lambda, \mathrm{T})\, C_{abs}(r, m, \lambda)\, d\lambda$$

Ratio of radiation flux from comet in visible–near infrared (i.e., the scattered radiation) to that in mid-infrared (i.e., thermal emission) can be interpreted in terms of albedo.

Notice that this albedo is average over the solar spectrum; whereas, typically single-scattering albedo ω is attributed to a fixed wavelength λ.

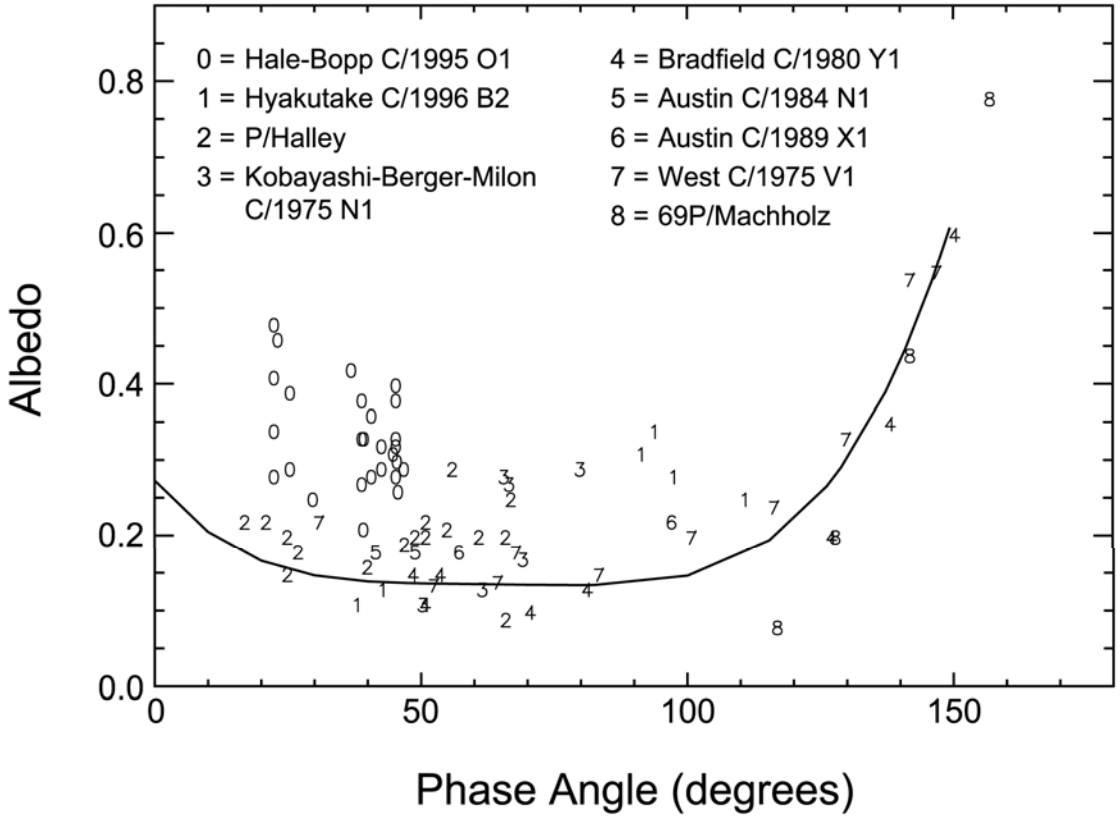

When observing an active far away from the comet (> 2 A.U.), particles consisting of water ice do not sublime quite rapidly. Therefore, in the near infrared, one can detect the absorption bands of water ice, namely, λ = 0.9 – 1.1 μm, 1.7 – 1.8 μm, 2.2 – 2.3 μm, and 3.08 μm.

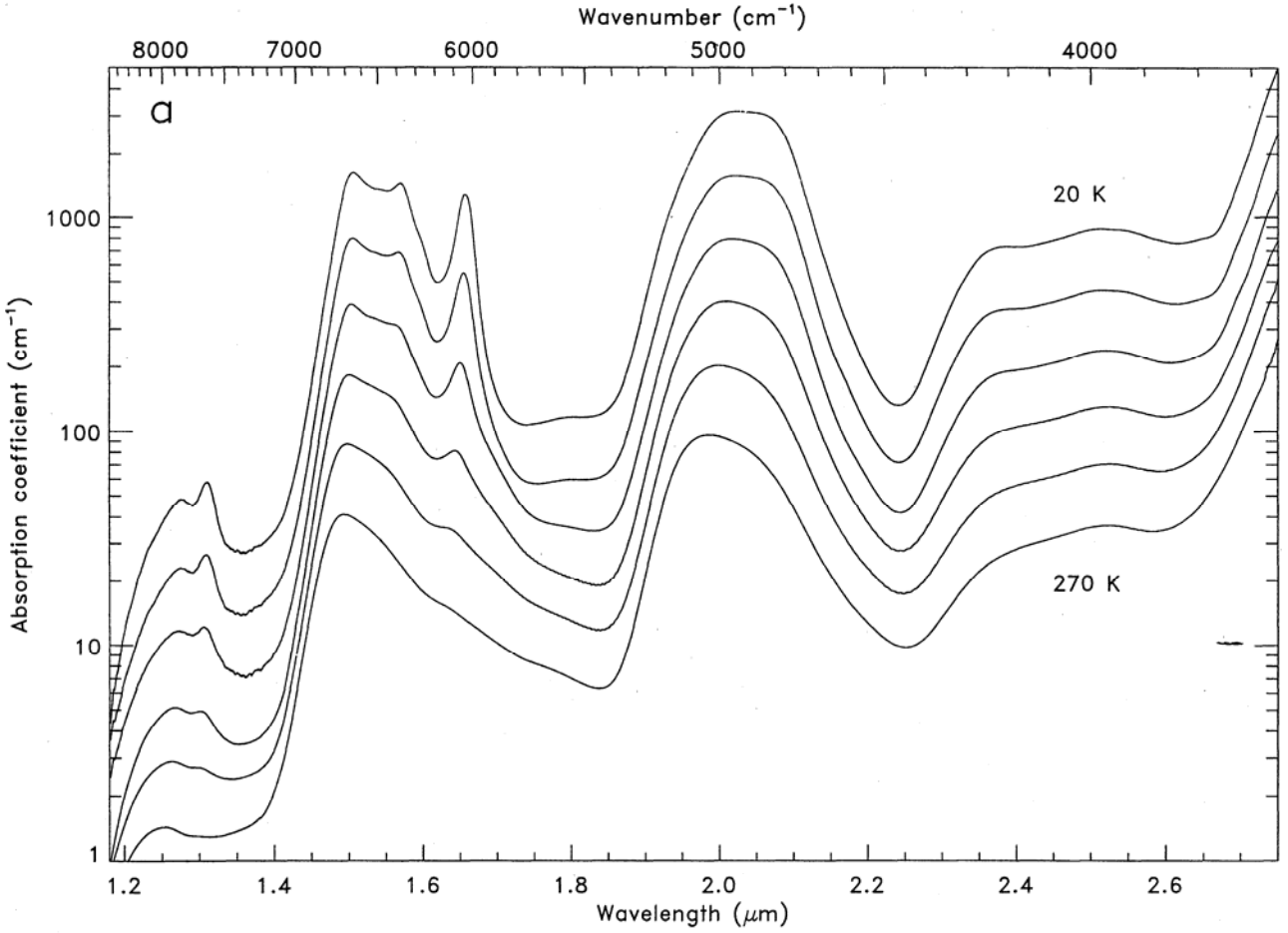

Water ice in comet 17P/Holmes at R = 2.4 A.U.

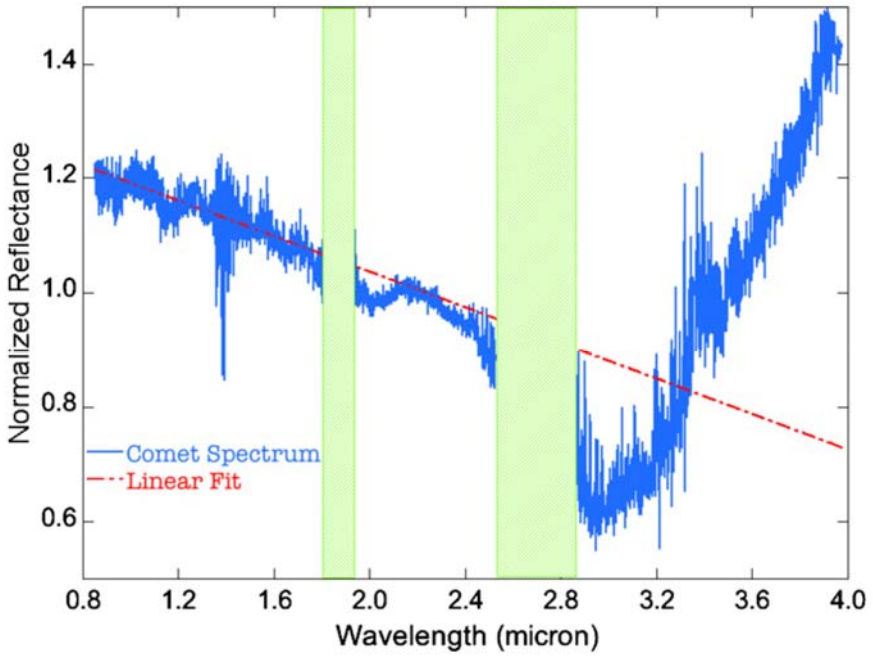

Figure Reflectance spectrum of 17P/Holmes from 0.8 to 4.0 μm, taken on UT 2007 October 27 and normalized at $\lambda = 2.2\ \mu m$. At shorter wavelengths ($\lambda < 3.0\ \mu$m), the most significant spectral feature of Holmes is the negatively sloped continuum. A linear fit to the continuum is shown as the red dashed line. The rising spectrum at wavelengths ($\lambda > 3.2\ \mu$m) is attributed to thermal emission. The two green shaded rectangles block out the regions that are heavily contaminated by the telluric absorptions.

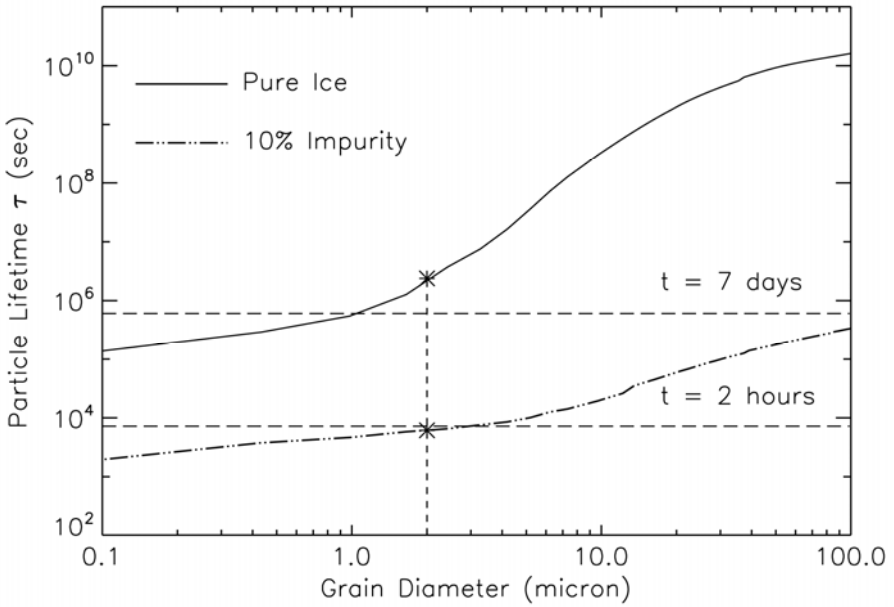

Figure Lifetimes of pure and dirty ice grains at the heliocentric distance of 2.45 AU. The two "star" symbols show the lifetimes of dirty (lower) and clean (upper) ice grains with a diameter of 2.0 μm. The lower horizontal dashed line indicates the required in-slit residence time which sets the lower limit of the lifetime for ice grains in the coma of 17P. It shows that only pure water ice was able to survive and to produce the detected absorption features. The upper horizontal dashed line represents the time interval between the start of the outburst and the end of our observations.

The 10-μm silicate emission feature

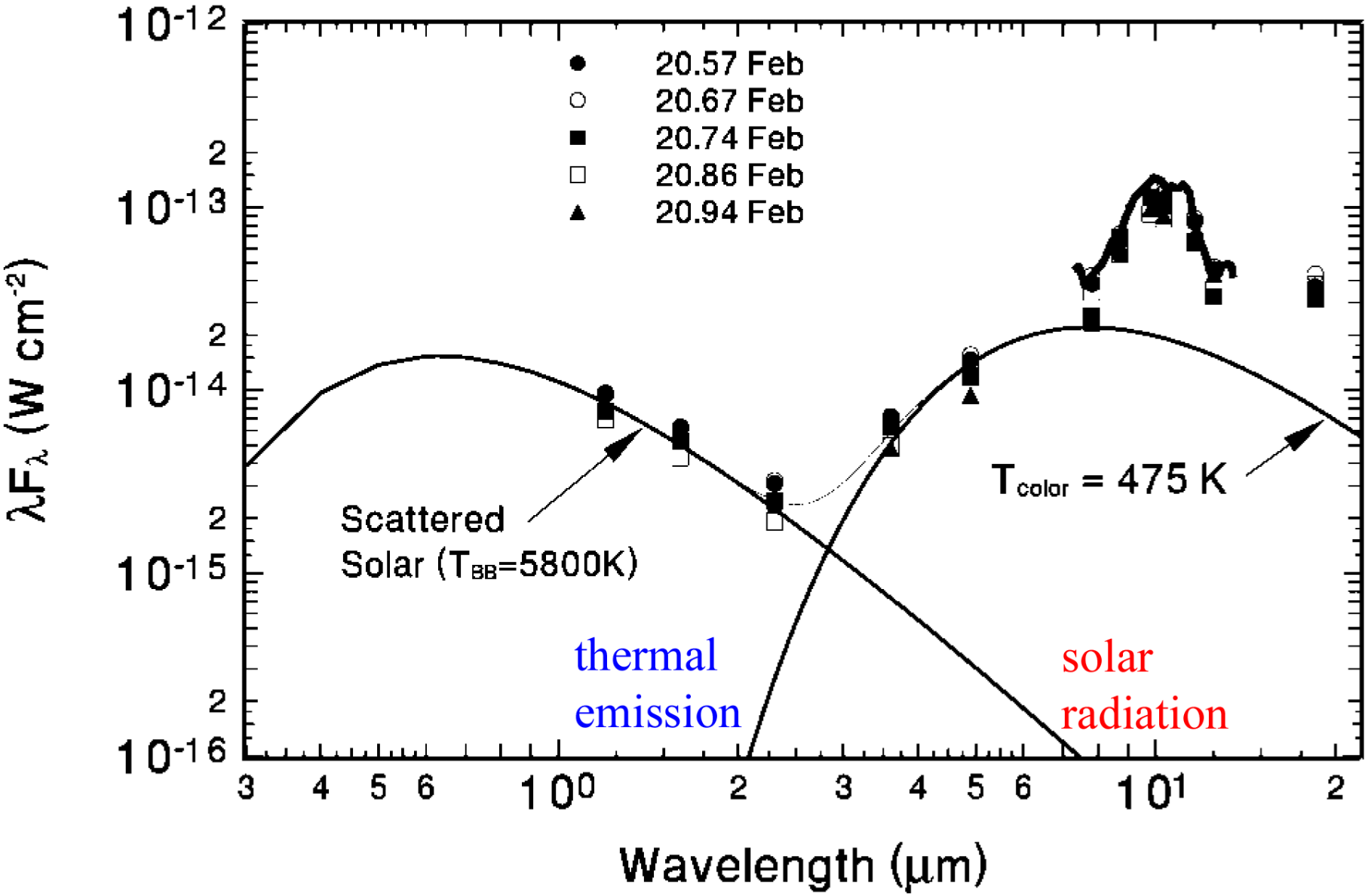

The 10-μm silicate emission feature

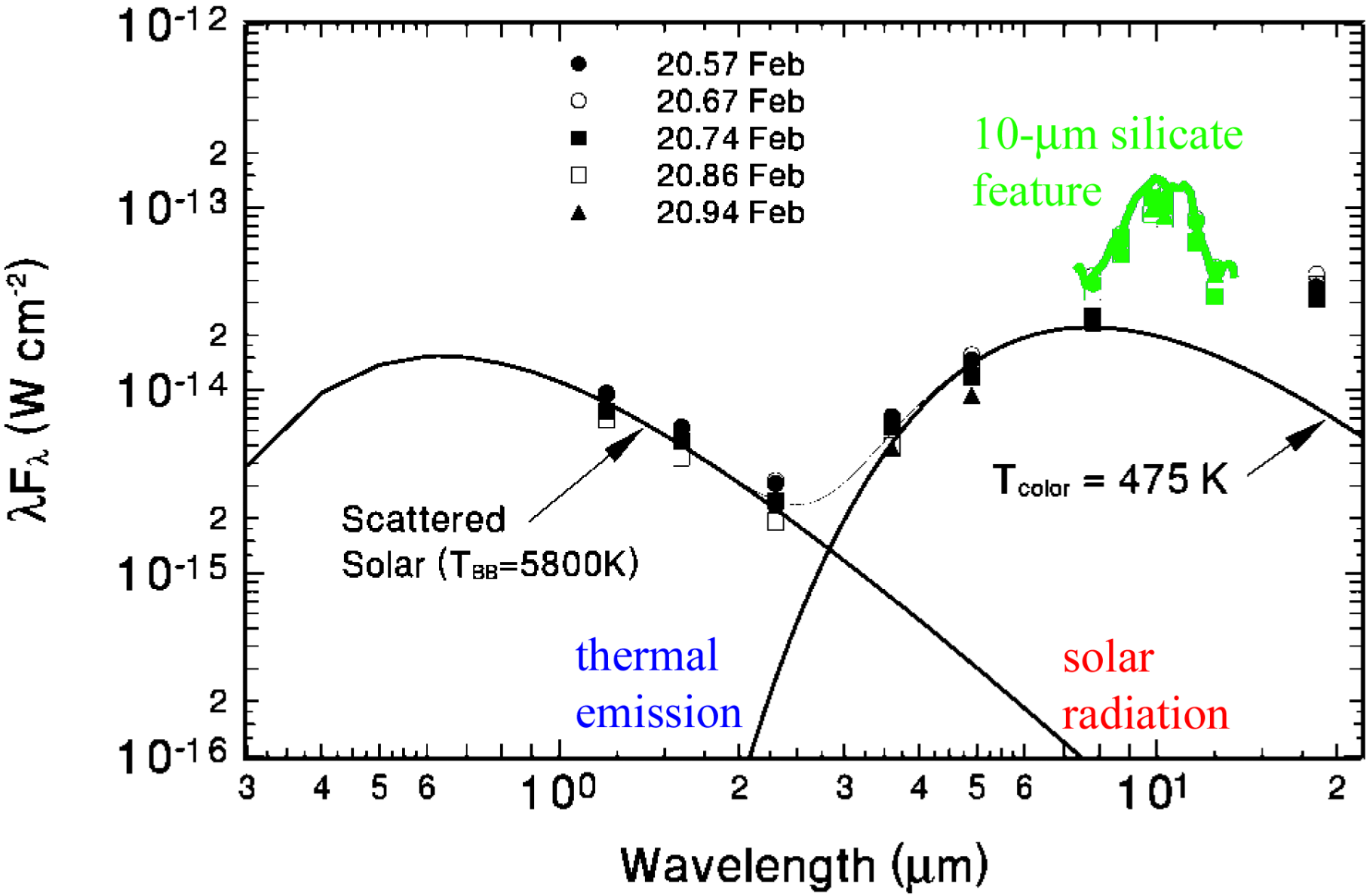

The 10-μm silicate emission feature

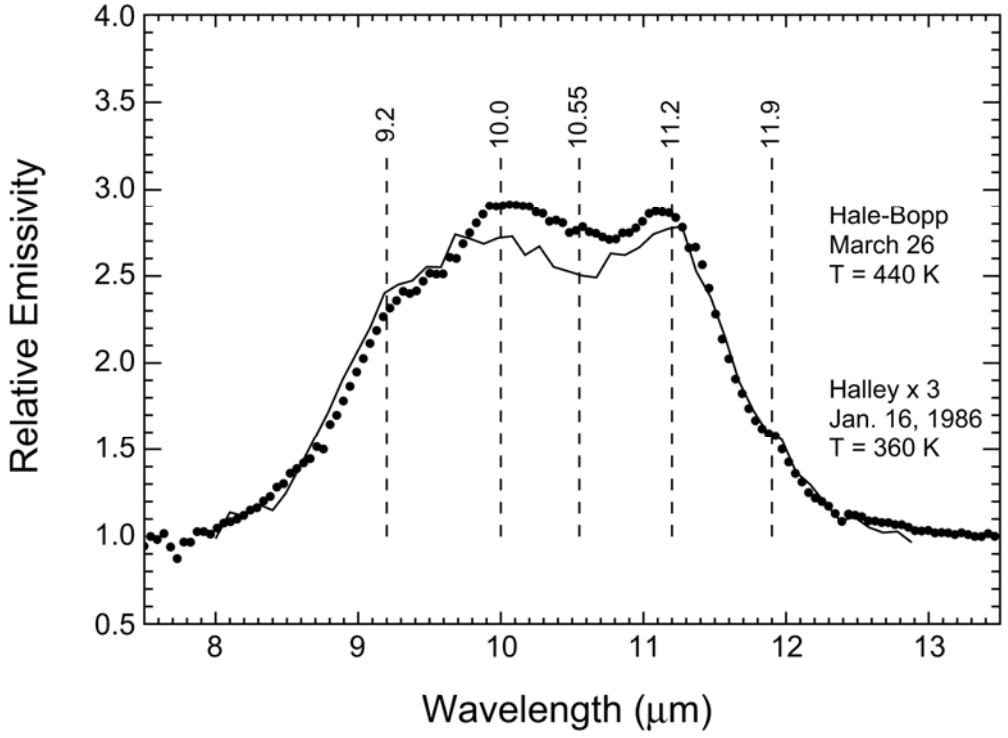

Fig. The 10-μm silicate emission feature in Hale-Bopp at r = 0.92 AU (dots) and 1P/Halley at r = 0.79 AU from *Campins and Ryan* (1989) (line). Each spectrum has been divided by a Planck function for the temperature shown and the Halley spectrum has been multiplied by 3. The spectral peaks in the Hale-Bopp spectrum are marked. From *Hanner et al.* (1999).

The 10-μm silicate feature may appear in the range from 8 to 13 μm.

It has three main peaks, at 9.2, 10.0, and 11.2 μm, and minor structure at 10.5 and 11.9 μm.

They are caused by stretching vibrations in Si–O bonds.

The 9.2-μm feature, first recognized in Hale-Bopp, is a signature of pyroxene ([Mg,Fe] SiO_3). A peak wavelength of 9.2 μm corresponds to amorphous, Mg-rich pyroxene; whereas, a peak near 9.3 μm is generally present in crystalline pyroxenes.

The broad 10-μm maximum in the cometary spectra is characteristic of amorphous olivine ($[Mg,Fe]_2$ SiO_4). However, crystalline olivine has a secondary peak at 10 μm as well.

Crystalline pyroxenes generate more variety in their spectra: peaks at 10–11 μm contribute to the width of the cometary feature and the structure near 10.5 μm.

The 11.2-μm peak is attributed to crystalline olivine ($[Mg,Fe]_2$ SiO_4), based on the good spectral match with the measured spectral emissivity of Mg-rich olivine. The 11.9-μm shoulder is also due to crystalline olivine.

Interestingly, the mass absorption coefficient of olivine near 11.2 μm is a factor of 3–10 times that of glassy silicates. Therefore, only a small fraction (15–20%) of the silicate material needs to be in the form of crystalline olivine to produce the observed peak.

Several comets display strong structured silicate emission with ratio of total flux to tontinuum at 10 μm exceeding 1.5. These include long-period comets C/1987 P1 (Bradfield), C/1990 K1 (Levy), C/1996 B2 (Hyakutake), and C/1995 O1 (Hale-Bopp), C/1993 A1 (Mueller), and 1P/Halley.

However, the strongest silicate emission was seen in comet C/1995 O1 (Hale-Bopp).

No strong 10-μm emission feature (20–25% above a black-body continuum) has yet been seen in a short-period comet.

Dependence of the silicate feature on heliocentric distance

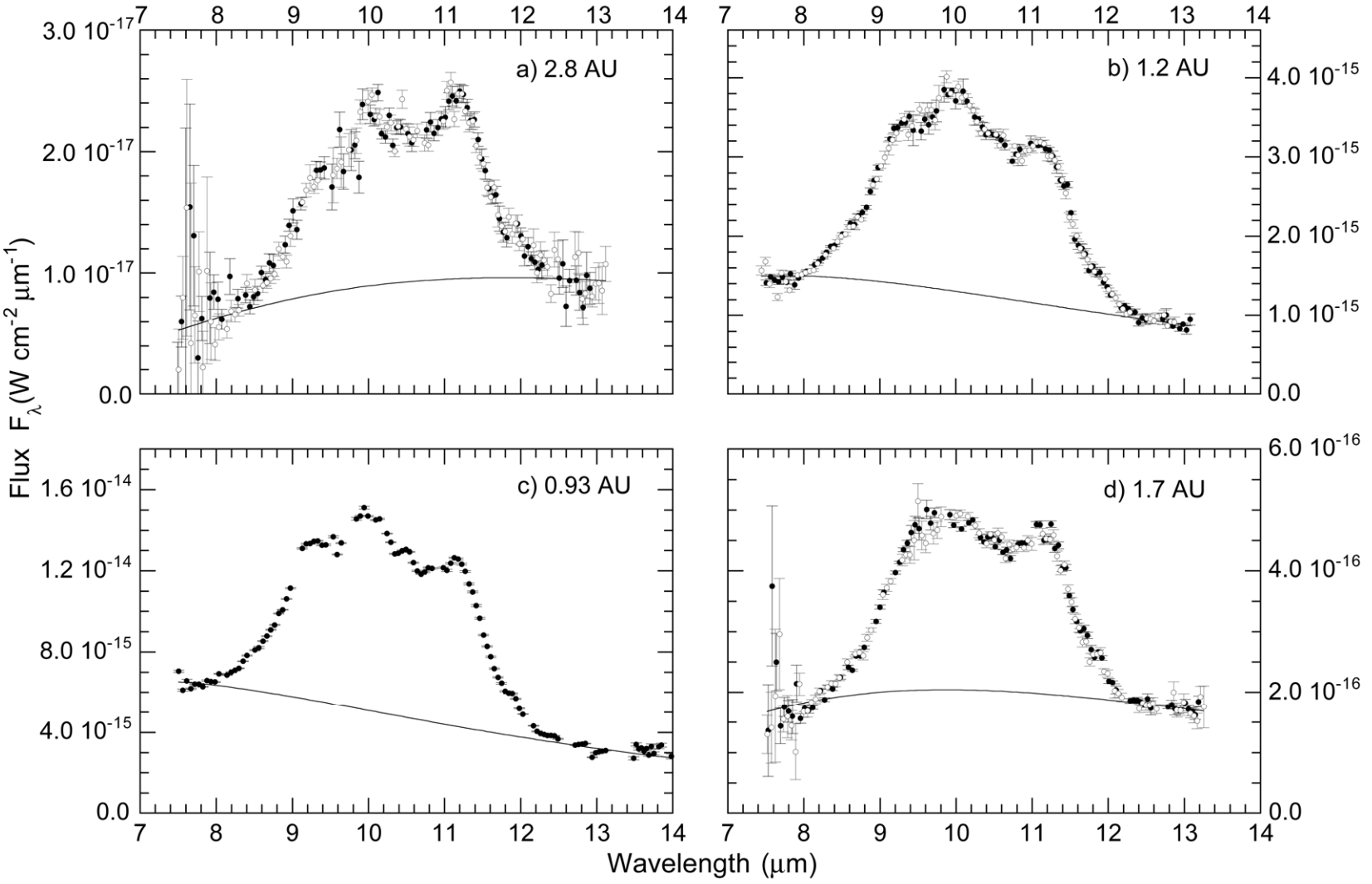

FIG. —Flux spectra of comet Hale-Bopp at four HIFOGS epochs at 2.8 AU (preperihelion), 1.2 AU (preperihelion), 0.93 AU (~perihelion), and 1.7 AU (postperihelion). (*a*) Co-added spectra taken at the same grating settings from 1996 October 11 UT and 1996 October 14 UT (*filled circles*) interlaced with co-added spectra from 1996 October 12 UT and 1996 October 13 UT (*open circles*). (*b*) Spectra from 1997 February 14 UT interlaced with 1997 February 15 UT, both taken during hour-long flare events on respective days. (*c*) Spectrum from 1997 April 11 UT. (*d*) Spectra from 1997 June 24 UT interlaced with 1997 June 25 UT. The multiplicative factors used scale the spectra prior to interlacing are given in Table 1. The 10 μm continuum blackbodies (*solid thin lines*) are fitted for $\lambda \leq 8.0$ μm and $\lambda \geq 12.4$ μm, with parameters given in Table 1.

“Absence” of the silicate feature in comet C/1996 Q1 (Tabur)

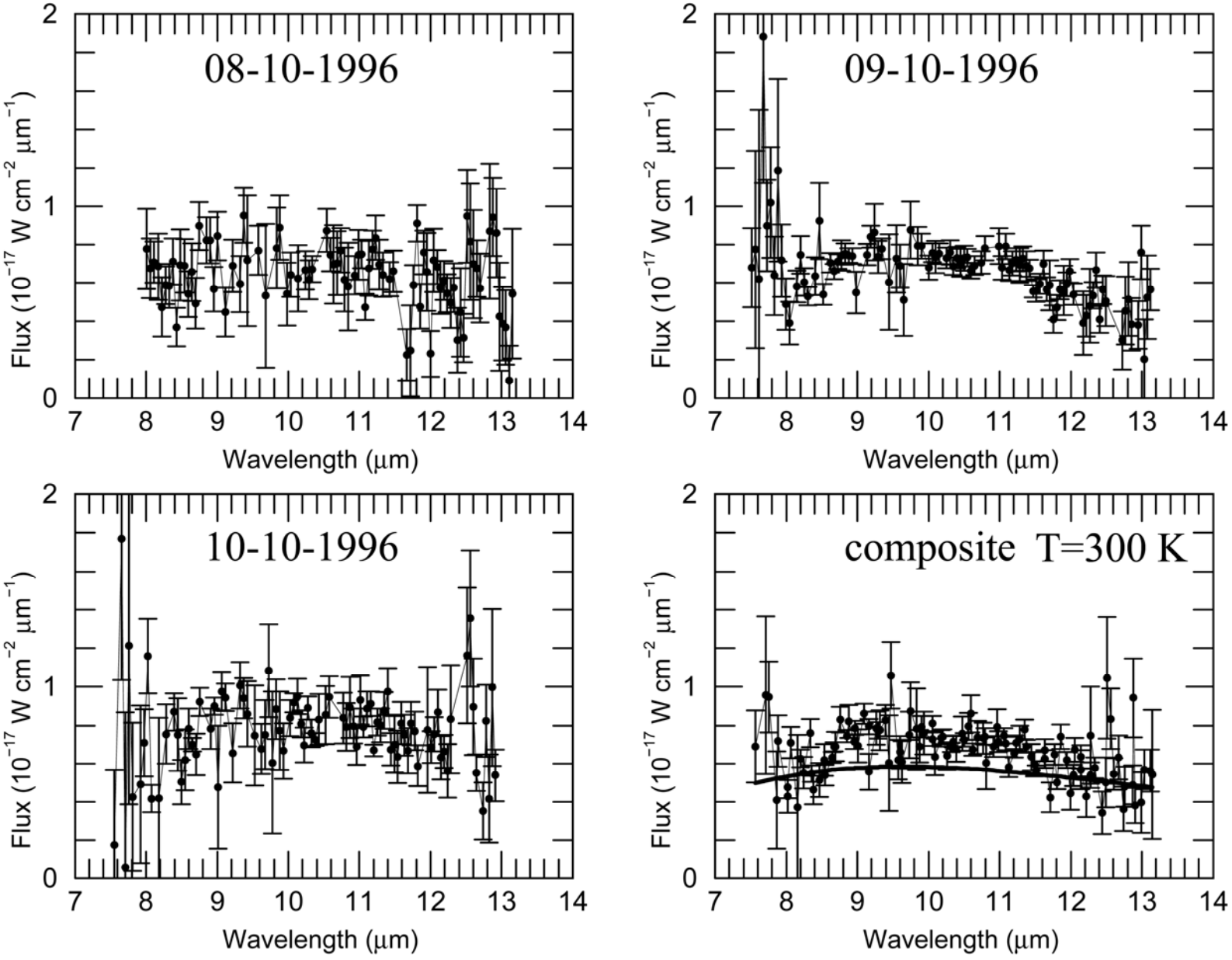

It is believed that in order to produce a strong emission feature, silicate particles must have radii on the order of 1 μm or smaller.

Larger particles will display a feature only if they are very porous aggregates and the individual constituent grains are micrometer-sized or smaller.

It is of high interest: where is the 10-μm silicate feature originated from in the coma? The answer to this question could be obtained from mid-infrared images of comets.

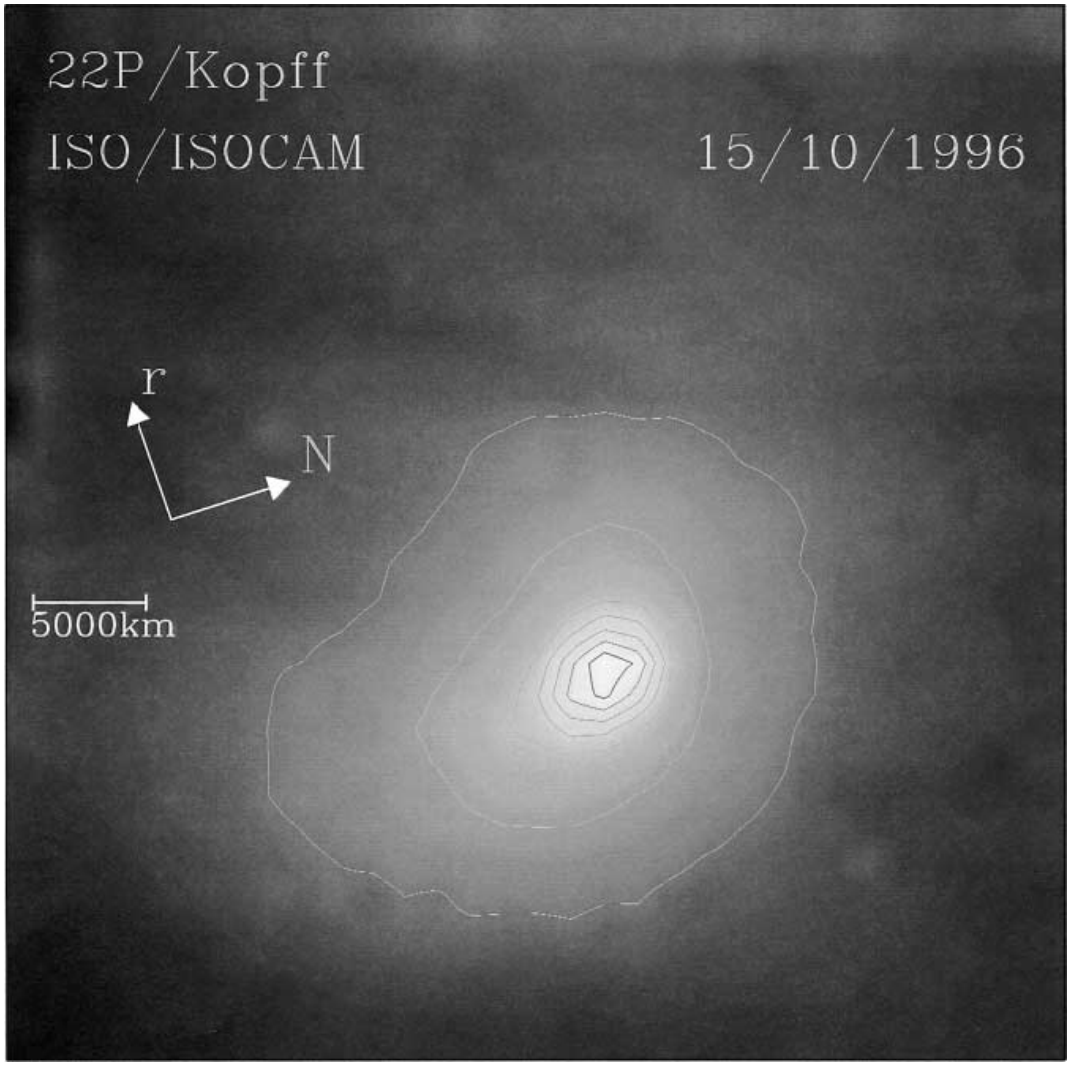

Broadband 11.5-μm image of comet 22P/Kopff taken in 15 October 1996. The arrows indicate the antisolar direction (vector r) and the direction of celestial North (N).

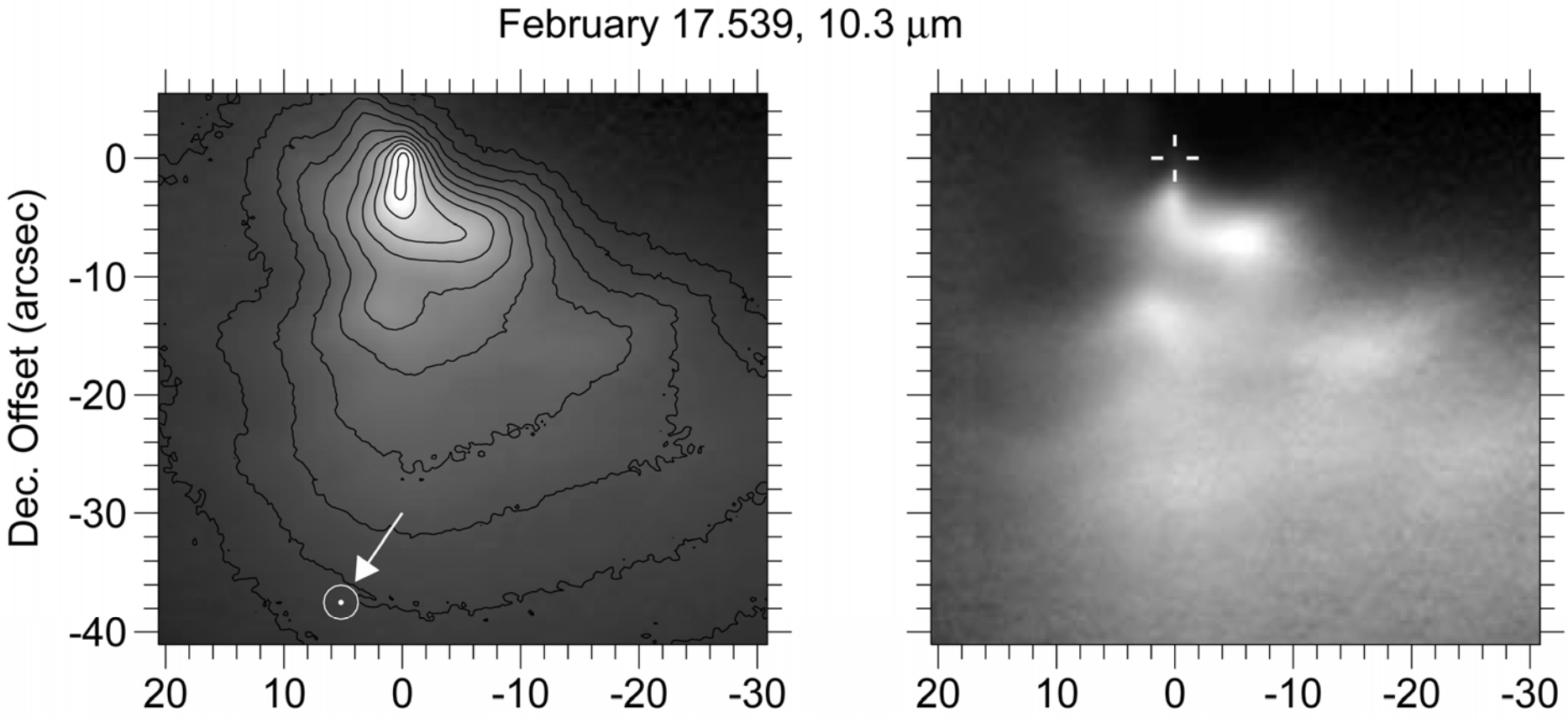

Mid-IR mosaics of comet C/1995 O1 (Hale-Bopp) taken in 1997. On the left column, original image with isophotes is shown; the ratio between isophotes is $\sqrt{2}$. The spatial scale is about 1200 km in 1 arcsec. On the right, images after dividing by a circularly symmetric function $1/\rho$, which enhances the jet and halos.

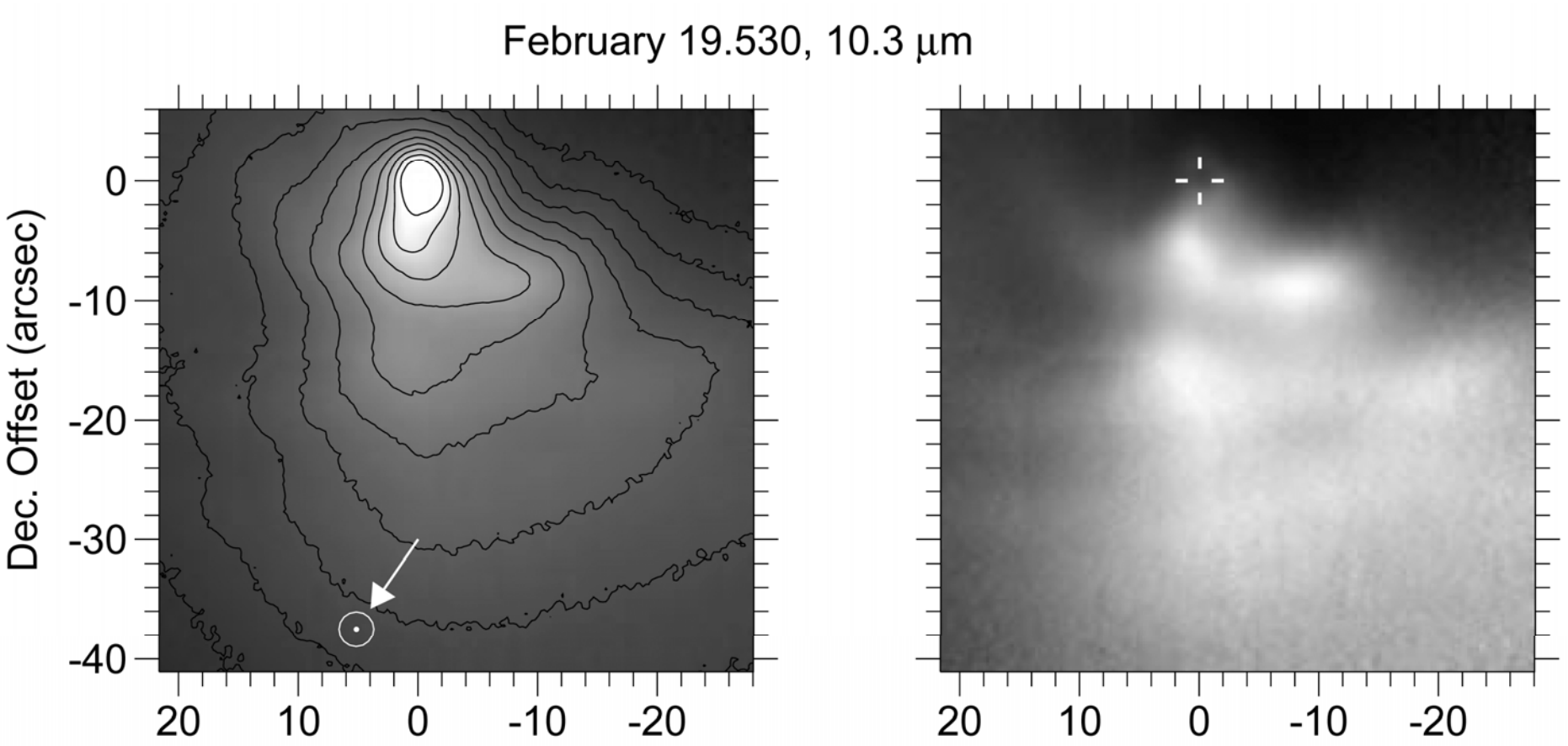

Mid-IR mosaics of comet C/1995 O1 (Hale-Bopp) taken in 1997. On the left column, original image with isophotes is shown; the ratio between isophotes is $\sqrt{2}$. The spatial scale is about 1200 km in 1 arcsec. On the right, images after dividing by a circularly symmetric function $1/\rho$, which enhances the jet and halos.

Spatially resolved Mid-IR spectra

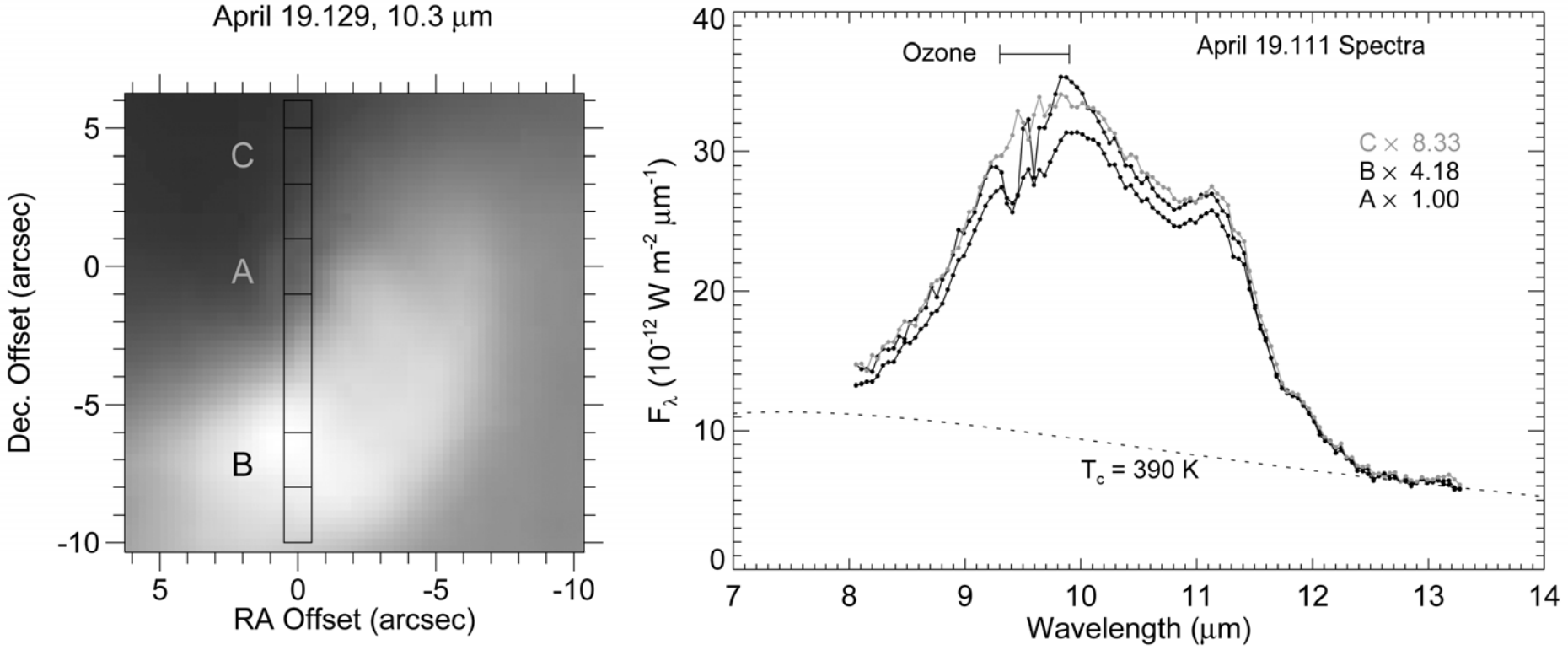

Mid-IR spectra of comet C/1995 O1 (Hale-Bopp) taken in 1997. Left panel presents the total intensity image with overlayed rectangles marking the spectrograph slit positions; whereas, right panel – individual spectra. Each label presents the scaling factors by which the data were multiplied to match at 12.8 μm.

Interpretation of IR spectrum of comet C/1995 O1 (Hale-Bopp)

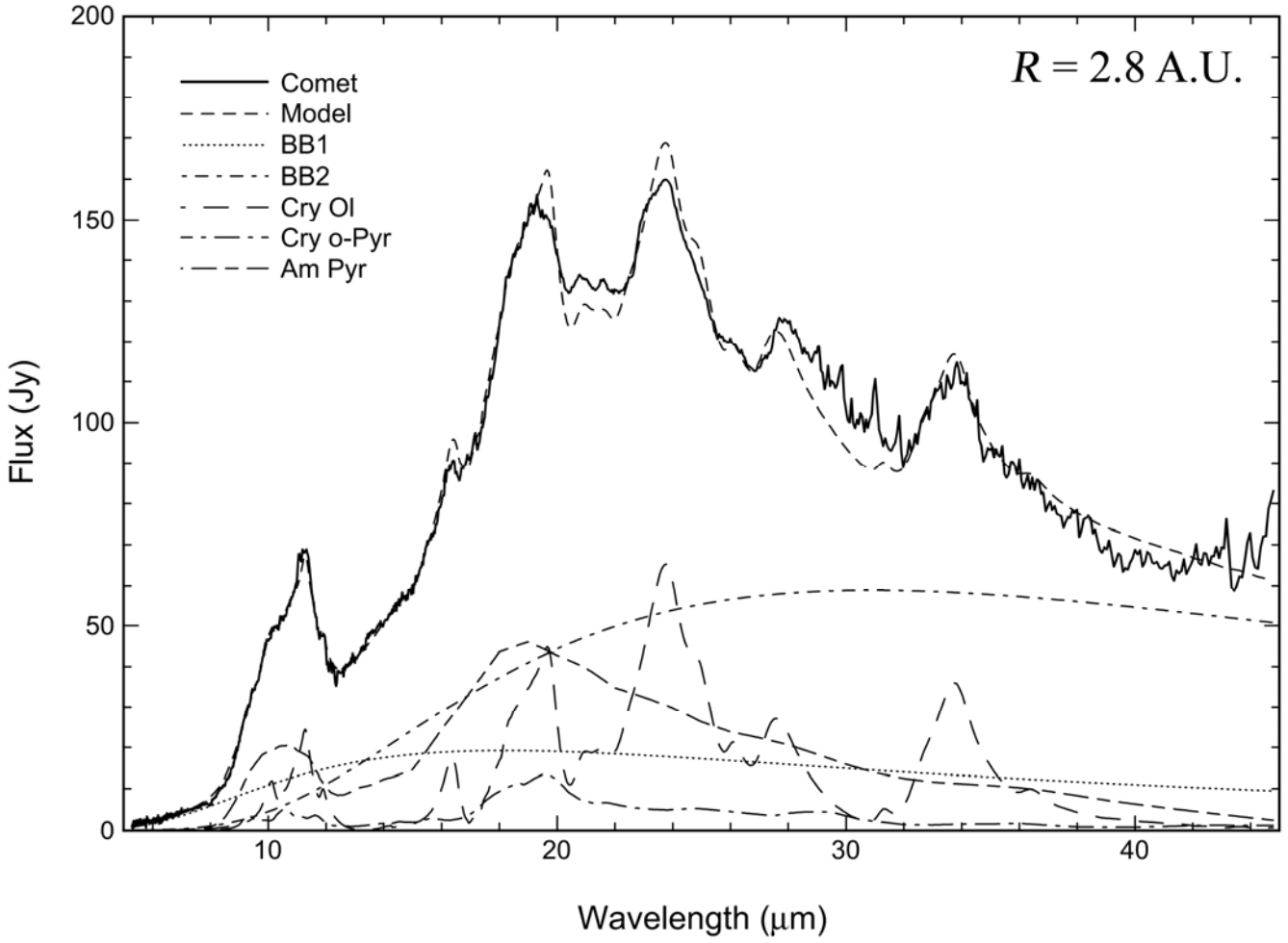

Five-component dust model: 280 K blackbody (BB1); 165 K blackbody (BB2); forsterite (Cry Ol 22%); orthopyroxene (Cry o-Pyr 8%); and amorphous pyroxene (Am Pyr 70%).

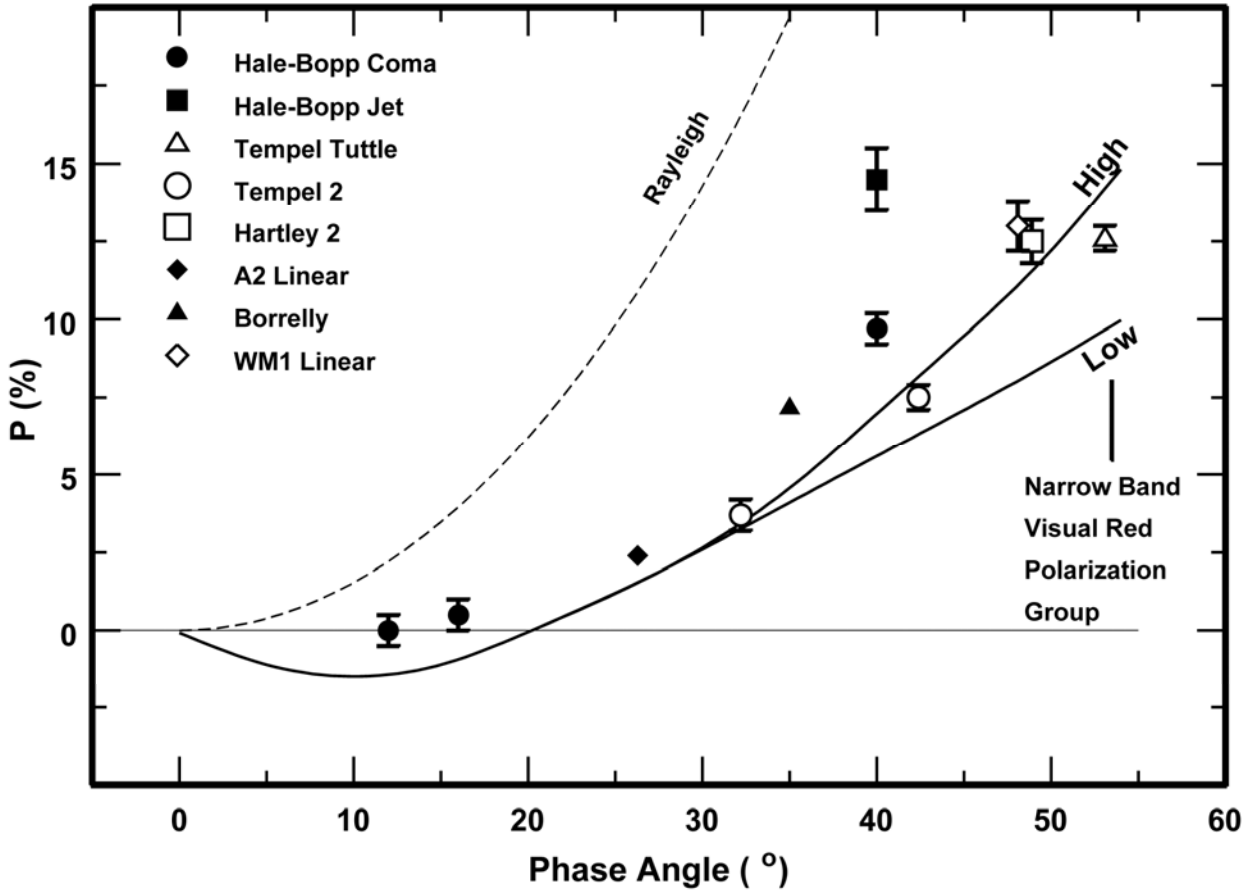

Polarization at 2.2 μm plotted against phase angle for six newly observed comets and C/1995 O1 (Hale-Bopp). The solid lines are the trend seen in the visual narrowband red for comets, which divides into two classes at phase angles larger than about 30°. The dashed line is the trend for pure Rayleigh scattering.

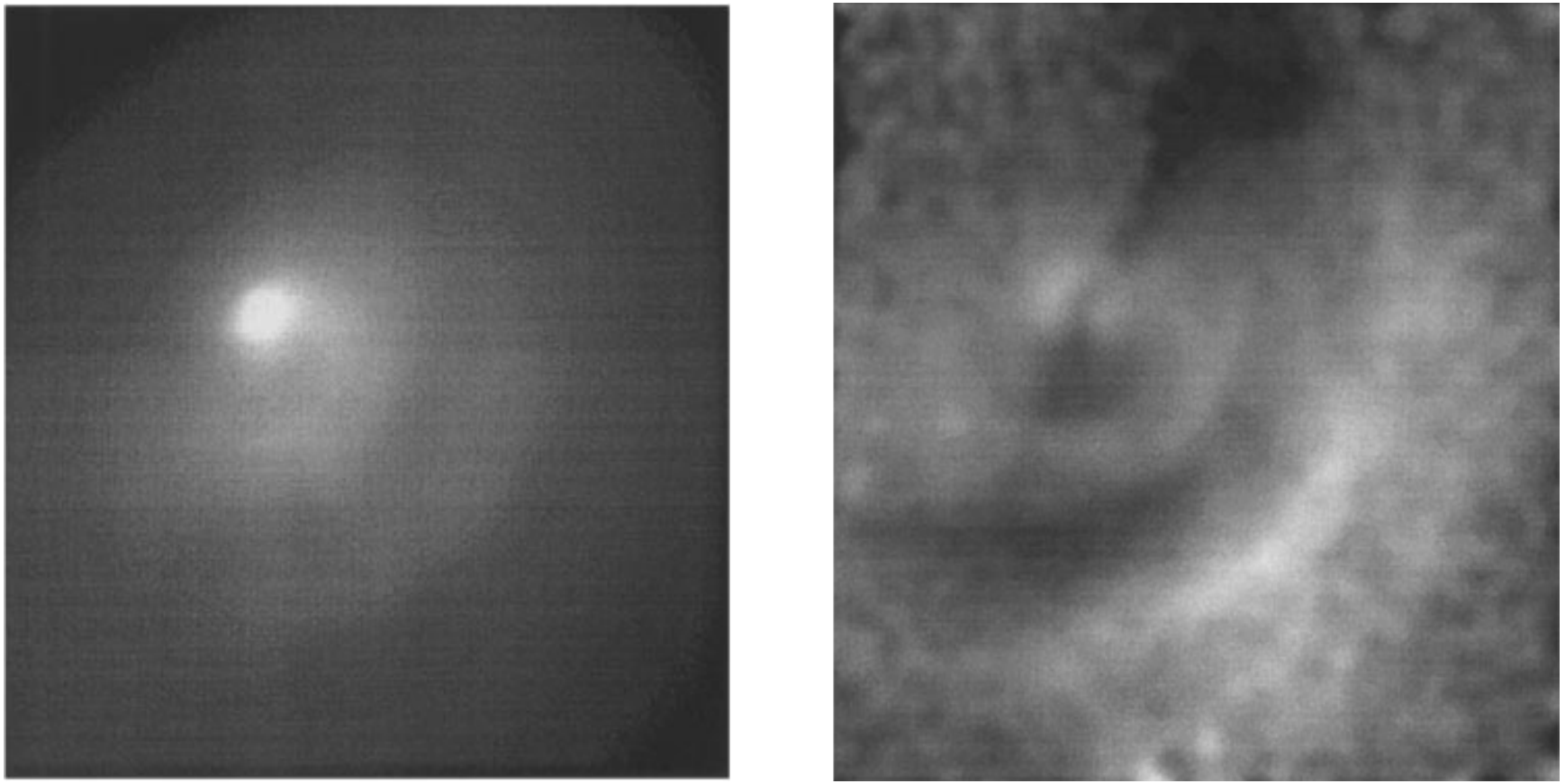

2.2-μm images of comet C/1995 O1 (Hale–Bopp) on 16.9 April, 1997, UT. Left panel presents intensity; whereas, right panel – linear polarization. The width of the frame is 74350 km; phase angle is of 39.6°. The dark areas correspond to 7% polarization, the bright areas to 11%. The dark streak running SE to NE is an artifact of the data analysis process.

References:

(1) Hanner, M.S., Bradley, J.P., (2004): in Comets II, M. C. Festou, H. U. Keller, and H. A. Weaver (eds.), 555–564.

(2) Kolokolova, L., et al., (2004): in Comets II, M. C. Festou, H. U. Keller, and H. A. Weaver (eds.), 577–604.

(3) Yang, B., Jewitt, D., Bus, S.J., (2009): Astron J, **137**, 4538–4546.

(4) Grundy, W.M., Schmitt, B., (1998): JGR, **103**, 25809–25822.

(5) Wooden, D.H., et al., (1999): Astrophys. J., **517**, 1034–1058.

(6) Harker, D.E., et al., (1999): Astron. J., **118**, 1423–1429.

(7) Lamy, P.L., et al., (2002): Icarus, **156**, 442–455.

(8) Hayward, T.L., et al., (2000): Astrophys. J., **538**, 428–455.

(9) Jones, T.J., Gehrz, R.D., (2000): Icarus, **143**, 338–346.